ACS central science

Research Article

Cite This: ACS Cent. Sci. 2019, 5, 789−795

http://pubs.acs.org/journal/acscii

Rapid Detection of *Salmonella enterica* via Directional Emission from Carbohydrate-Functionalized Dynamic Double Emulsions

Lukas Zeininger,[†] Sara Nagelberg,[‡] Kent S. Harvey,[†] Suchol Savagatrup,[†] Myles B. Herbert,[†] Kosuke Yoshinaga,[†] Joseph A. Capobianco,[§] Mathias Kolle,*[,‡] and Timothy M. Swager*[,†]

[†]Department of Chemistry and [‡]Department of Mechanical Engineering, Massachusetts Institute of Technology, Cambridge, Massachusetts, United States

[§]Agricultural Research Service, United States Department of Agriculture, Wyndmoor, Pennsylvania, United States

Supporting Information

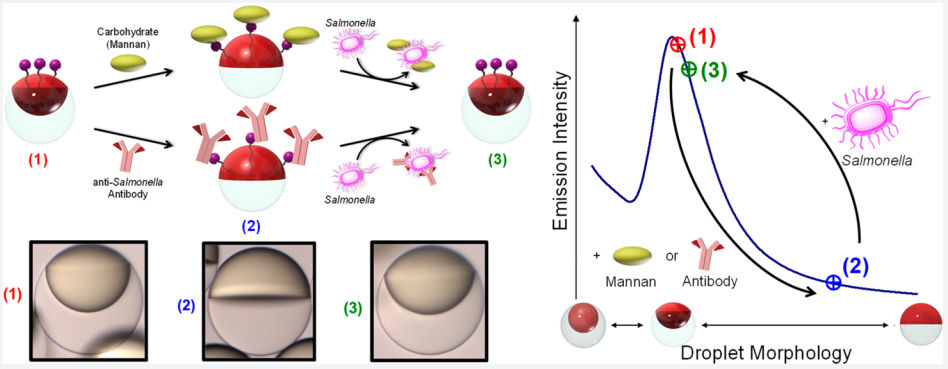

ABSTRACT: Reliable early-stage detection of foodborne pathogens is a global public health challenge that requires new and improved sensing strategies. Here, we demonstrate that dynamically reconfigurable fluorescent double emulsions can function as highly responsive optical sensors for the rapid detection of carbohydrates fructose, glucose, mannose, and mannan, which are involved in many biological and pathogenic phenomena. The proposed detection strategy relies on reversible reactions between boronic acid surfactants and carbohydrates at the hydrocarbon/water interface leading to a dynamic reconfiguration of the droplet morphology, which alters the angular distribution of the droplet's fluorescent light emission. We exploit this unique chemical−morphological−optical coupling to detect *Salmonella enterica*, a type of bacteria with a well-known binding affinity for mannose. We further demonstrate an oriented immobilization of antibodies at the droplet interface to permit higher selectivity. Our demonstrations yield a new, inexpensive, robust, and generalizable sensing strategy that can help to facilitate the early detection of foodborne pathogens.

INTRODUCTION

Foodborne diseases are a major worldwide public health concern. Each year, approximately 48 million people in the United States (around one-sixth of the population) become ill as a result of consuming pathogen-contaminated food or water that causes serious symptoms and even death.[1] In addition, this leads to an annual economic burden of more than 55.5 billion dollars due to premature deaths, lost work days, and health care expenses.[2,3] Infections by *Salmonella enterica*, a species of Gram-negative bacteria commonly found in poultry, account for nearly a quarter of all annual cases of foodborne illness. Unfortunately, commonly used methods to detect *Salmonella* lack the sensitivity that is necessary to directly detect the small number of pathogenic cells that can cause illness. Instead, these approaches require incubation steps that can take up to 48 h,[4,5] a timespan that can be critical in treating patients with foodborne illness or preventing further spread and consumption of contaminated food products. New methods that can rapidly detect miniscule amounts of pathogenic cells, ideally within a single 6-h work shift at a food production plant, are therefore urgently needed to efficiently prevent contaminated food from reaching consumers and causing widespread diseases.

The need for distributed real-time foodborne pathogen detection has led to increased scientific activity in chemical and biological sensor development and has fueled innovations in new sensory materials.[6−8] In this context, liquid−liquid transduction schemes, such as oil-in-water emulsions, are especially appealing, because the hydrophobic−hydrophilic liquid interfaces are dynamic and closely resemble the environment found at a cell's surface.

RESULTS AND DISCUSSION

Herein, we demonstrate a new emissive sensor scheme based upon the dynamic nature of liquid multicompartment

Received: January 19, 2019
Published: April 23, 2019

DOI: 10.1021/acscentsci.9b00059
ACS Cent. Sci. 2019, 5, 789−795

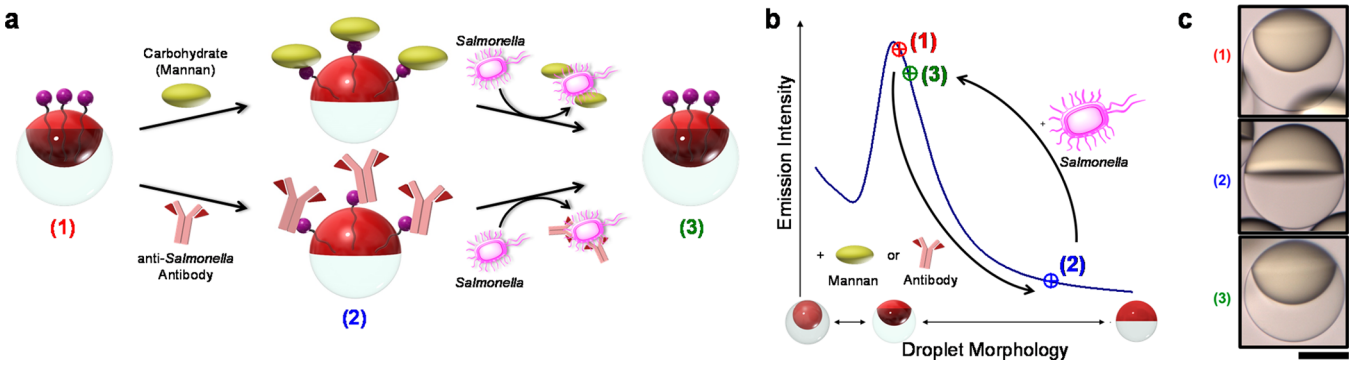

Figure 1. Conceptual sketch of the mechanism for the detection of *Salmonella enterica* cells using boronic acid-functionalized complex emulsions with reversible assembly of carbohydrate or IgG antibody. (a) Changes in the droplet morphology, induced by reversible assembly of carbohydrates or IgG antibodies at the hydrocarbon (HC, red) water (W) interface and upon removal by competitive binding to *Salmonella* cells. (b) Light-curve: Boronic acid-functionalized emulsions are initialized to yield the highest emission intensity (1); upon reversible binding to carbohydrates or antibodies the emission intensity decreases by up to 60% resulting from the reconfiguration to the Janus morphology (2); the emission intensity transitions back to the high original state upon removal of the carbohydrates or antibodies by *Salmonella* cells (3). (c) Side-view images of droplets (scale bar, 50 μm) in the three morphology states characteristic for the light-curve: (1) starting point: droplets containing boronic acid surfactant in 100% Zonyl surfactant solution (2) after addition of 30 μg mL^{-1} of the carbohydrate mannan, and (3) after addition of 10^5 cells mL^{-1} *Salmonella typhimurium* cells.

emulsions that consist of two immiscible phases with a large refractive index (n) contrast, a hydrocarbon oil (HC, red; n_{HC} = 1.49), and a fluorocarbon oil (FC, white; n_{FC} = 1.29) (Figure 1a). Polydisperse and monodisperse complex droplets with these solvents are readily obtained by emulsification in an aqueous solution containing surfactants (W; n_W = 1.33), using a temperature-induced phase separation method.[9,10] The morphology of these complex emulsions can be dynamically switched between encapsulated (HC/FC/W and FC/HC/W) and Janus configurations in response to changes in the type, concentration, and configuration of surrounding surfactants.[11,12]

Biomolecular recognition events can generate changes in droplet configuration (Figure 1a), and we quantify these effects by measuring distinct changes in directional emission as the sensing output. To create an optical read-out that is sensitive to small changes in the droplet morphology, a fluorescent perylene dye is localized in the higher refractive index hydrocarbon phase. As a result of the higher refractive index of the hydrocarbon phase, total internal reflection confines the perylene emission. The light emission characteristics of these multicompartment droplets are strongly dependent on the droplets' interfacial curvatures and refractive index contrast. The intensity of light emitted in the direction normal to the sample surface varies as a function of droplet morphology as defined by the "light-curve" (L-curve) in Figure 1b.

To invoke a dynamic reconfiguration of the droplets' morphology in response to the presence of micro-organisms, we employed boronic acid surfactants that reversibly bind mono- and polysaccharides, as well as N-glycans present in IgG antibodies. Changes in the HC/W interfacial tension associated with reversible interfacial reactions between the boronic acids and these recognition groups are detected optically. These optically readable and chemically triggered droplet morphology changes were then used to create a hitherto unknown, rapid, and sensitive method for the detection of the foodborne pathogen *Salmonella enterica* serovar Typhimurium (Figure 1b,c).

To understand the underlying optical phenomena, the emission of dyed complex emulsions was modeled using raytracing techniques. The calculations revealed a strong dependence of the anisotropic angular intensity distribution on changes in the droplet morphology (Figure 2a,b). To approximate a continuous fluorescing medium, we initialized 20 000 000 rays per unit volume with homogeneous and randomized starting directions, locations, and polarizations within the HC-phase. Individual ray trajectories were determined using a custom nonsequential raytracing algorithm in MATLAB, and the intensity of the output rays was collected to 1° bins. Light rays that intersect the internal HC/FC interface at an angle less than the critical angle for total internal reflection, $\theta_c = \sin^{-1}(n_{FC}/n_{HC}) = 60°$, are simply treated as background emission. Rays intersecting the internal interface at an angle larger than θ_c are guided along the interface by total internal reflection, until they encounter the HC/W interface, where they escape the droplet near the three-phase contact line at a morphology-dependent angle. Calculations show that large changes in emission intensity can be measured in the vertical direction (0°) of gravity-aligned emulsions.

We verified this morphology-dependent emission of the complex emulsions experimentally by taking optical micrographs of fluorescent droplets. We observed the predicted dominant emission along the gravitational axis that appears as a bright ring at the three-phase junction (Figure 2c and Figure S1). Large variations in the light intensity at the three-phase junction indicate the location where light that undergoes total internal reflection (TIR) exits the droplet. The experimentally measured variations in the intensity of light emitted normal to the sample surface (Figure 2d) as a function of droplet morphology agree well with the computed morphology-dependent variations of the droplets' emission (Figure 2e).

We measured the quantitative read-out of changes in droplet morphology by positioning a bifurcated fiber connected to a light source and a spectrometer vertically above a monolayer of the emulsions (emission direction = 0°) (Figure 2d). In this configuration, the fiber was used for both excitation (λ = 400 nm) and collection of emitted light (λ = 475 nm). The L-curve in Figure 2e displays the normalized intensity of light emitted in the normal direction of the sample surface by gravity-aligned droplets as a function of morphology adjusted by the ratio of hydrocarbon (SDS) and fluorocarbon (Zonyl FS-300) surfactants in the aqueous phase. We used the contact angle

DOI: 10.1021/acscentsci.9b00059
ACS Cent. Sci. 2019, 5, 789−795

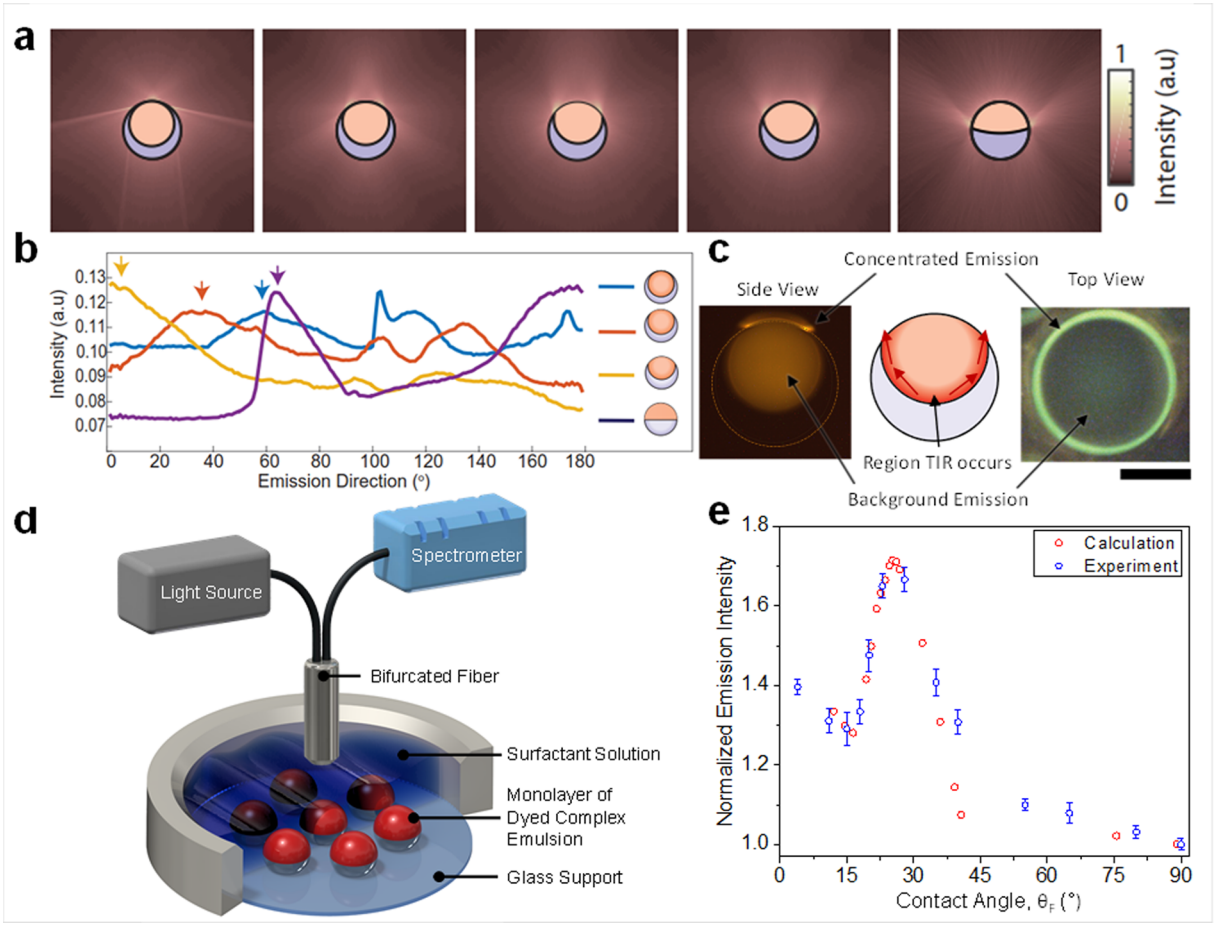

Figure 2. Directional light emission from complex emulsions. (a) Intensity distribution around the droplet determined by 2D raytracing for varying droplet morphologies. (b) Computationally determined emission intensity in the far field as a function of polar angle measured from the droplets' symmetry axis by full 3D raytracing. Arrows indicate the TIR light out-coupled at the three-phase junction. (c) Side-view diagram showing region of TIR (middle) and top- and side-view fluorescence optical micrographs of an emissive emulsion (scale bar, 50 μm) in state where the TIR light is directed sideways (left) and upward (right) showing the higher light intensity near the three-phase contact line. (d) Experiment for the measurement of the emission intensity as a function of droplet morphology, including a bifurcated fiber used for both excitation (λ= 400 nm) and collection of emitted light intensity (λ= 475 nm). (e) Light-curve: Calculated and measured emission intensities as a function of the contact angle at the three-phase junction above a gravity-aligned droplet monolayer, wherein the emission intensity of droplets in the Janus configuration (contact angle = 90°) was normalized to 1.0.

(θ_F) of the three-phase junction, as determined by side-view images of the respective droplet configurations obtained for each surfactant ratio, to quantify the droplet morphology (Figure S2).[13]

In the limiting case of a fully encapsulated HC in FC double emulsion (HC/FC/W, θ_F = 0°), the optical field can extend via frustrated total internal reflection across the thin interface at the top of the droplet and light leaks out. After slightly "opening up" of the droplet and exposing of the HC/W interface, TIR light can exit the droplet. Variations in droplet morphology, quantified by θ_F, lead to changes in the angle at which the TIR light escapes the emulsions. We observed a local minimum in the vertical emission intensity with the morphology for which the TIR light is emitted horizontally outward ($\theta_F \approx 16°$). Further increase in θ_F (and the expansion of the HC/W interface) results in an increase of the light intensity until a maximum is reached (θ_F = 25°), which corresponds to the morphology where the majority of totally internally reflected light is directed in the vertical direction (third image of Figure 2a,c). Upon passing the maximum, increases in contact angle result in a pronounced decrease in the emission intensity as the droplet morphology progresses to the Janus state. Figure 2e reveals the excellent agreement between experimentally observed light intensities and theoretical predictions, wherein we modeled and integrated the intensity of light emitted in a cone matching the collection fiber's numerical aperture (NA = 0.22) and orientation.

The L-curve in Figure 2 enables a new versatile sensing paradigm for the rapid and sensitive detection of carbohydrates and *Salmonella* bacteria. To create L-curve sensors, we designed responsive boronic acid surfactants that modulate the interfacial tension through reversible binding of carbohydrate cis-diols. Boronic acids are well-established receptors for this class of biomolecules, and a variety of molecular sensors that exhibit selectivity for higher saccharides and other glycosylated biomolecules have been reported.[14−16] However, boronic acid-based molecular sensors have seen limited utility in the native aqueous biosensing conditions.[17,18] In this context, the dynamic hydrophobic−hydrophilic liquid interfaces of complex emulsions represent an attractive platform to facilitate reactions between boronic acid surfactants and carbohydrates at the HC/W interface to induce analyte-

DOI: 10.1021/acscentsci.9b00059
ACS Cent. Sci. 2019, 5, 789−795

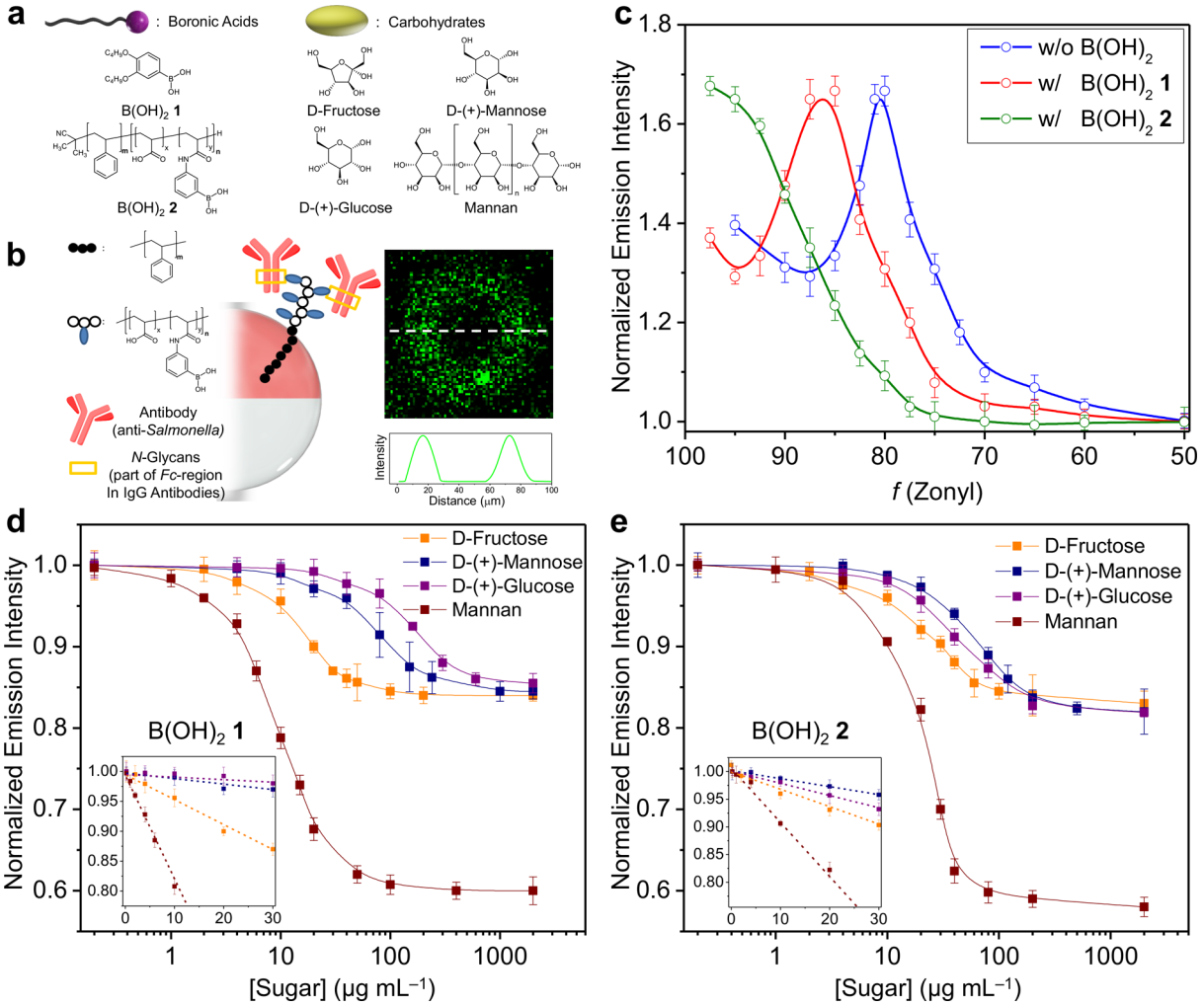

Figure 3. Carbohydrate sensing and antibody attachment to boronic acid-functionalized complex emulsions. (a) Chemical structures of boronic acid surfactants and carbohydrates used in this study. (b) Schematic illustration of the oriented attachment of IgG antibodies (25 μg mL^{-1}) at the HC/W interface of complex emulsions using B(OH)$_2$ **2** and confocal optical micrograph of a droplet functionalized with a dye(FITC)-labeled IgG antibody. (c) Shifts in the L-curve upon the additions of the boronic acid surfactants **1** and **2**. (d, e) Normalized emission intensity as a function of mono- and polysaccharide concentrations and standard deviations ($N \geq 5$) for droplets functionalized with B(OH)$_2$ **1** (d) and B(OH)$_2$ **2** (e). Insets show the slope of the linear decrease of the emission intensity at low sugar concentrations that can be correlated to the effectiveness of the sugars for lowering the HC/W interfacial tension.

dependent variations in the interfacial tension. To this end, we employed two boronic acid cosurfactants, 3,4-dibutoxyphenylboronic acid (B(OH)$_2$ **1**)[19] and polystyrene-*block*-poly(acrylic acid-*co*-acrylamidophenylboronic acid) (B(OH)$_2$ **2**),[20] which localize at the HC/W interface (Figure 3a). Implementation requires adjusting the droplet morphology to produce a maximum emission intensity by balancing the concentration of the boronic acid cosurfactants in the hydrocarbon phase and Zonyl in the water phase. B(OH)$_2$ **1** and **2** behave as surfactants, and the maximum emission intensity peak on the L-curve shifts to higher Zonyl/SDS ratios (i.e., less SDS is needed), as shown in Figure 3c. We define this state as the "active" state, wherein the highest amount of emitted light is directed into the collection fiber.

Changes in carbohydrate concentration are detected by monitoring changes in the vertical emission intensity, which varies with miniscule changes in the droplet morphology. Decreases in the emission intensity upon addition of fructose, glucose, and mannose to B(OH)$_2$ **1**-functionalized droplets (Figure 3d) reflect the differing binding constants between the monosaccharides and phenyl boronic acids.[21,22] At low sugar concentrations (below 50 μg mL^{-1}), the calibration curves for these simple sugars are relatively linear and provide precise detection of fructose (R^2 = 0.982), glucose (R^2 = 0.991), and mannose (R^2 = 0.980) (inset in Figure 3d). Similarly, the addition of monosaccharides to droplets containing B(OH)$_2$ **2** resulted in a decrease of the emission intensity as a function of morphology (Figure 3e). However, the differences had less dependence on the expected binding affinities, which is likely the result of multiple binding interactions of the polymeric B(OH)$_2$ **2** surfactant. We also obtained linear calibration curves for fructose (R^2 = 0.983), glucose (R^2 = 0.997), and mannose (R^2 = 0.994) for B(OH)$_2$ **2**-containing droplets at low monosaccharide concentrations (inset in Figure 3e). Mannan, a polymer of β-1,4-linked mannose subunits, produces significantly larger changes in droplet morphology (<30 μg mL^{-1} to produce a maximum decrease in the emission intensity) as a result of its increased size, hydrophilicity, and multivalency.

DOI: 10.1021/acscentsci.9b00059
ACS Cent. Sci. 2019, 5, 789−795

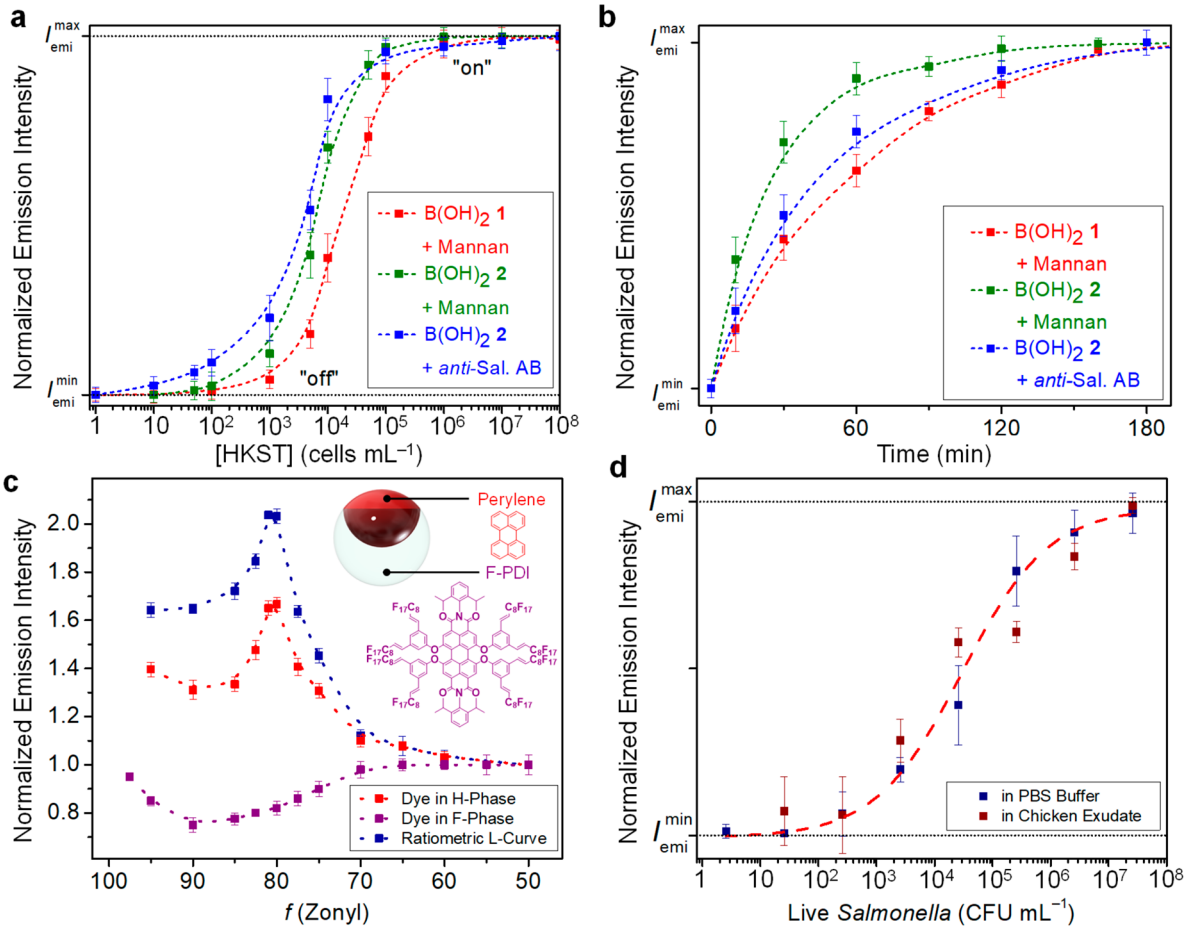

Figure 4. Detection of *Salmonella enterica* cells using carbohydrate- or antibody-functionalized complex emulsions. (a, b) Measured emission intensity and standard deviations ($N \geq 5$) as a function of *Salmonella* cell concentration (a) and time (detection of 10^5 HKST mL^{-1}) (b). (c) Normalized emission intensities of polydisperse droplets containing perylene dye in the H-phase (λ = 475 nm) and a fluorinated perylene diimide dye in the F-phase (λ = 580 nm). The ratio between the two emissions was used as a ratiometric read-out for the detection of live *Salmonella* bacteria. (d) Ratiometric emission intensity as a function of the concentration of live *Salmonella* bacteria in PBS solution and in chicken exudate.

We leveraged this reversible binding of carbohydrates that alters the droplet morphology for the detection of foodborne pathogens. Selective interactions between carbohydrates and bacteria cells have been reported previously.[23−25] We targeted *Salmonella enterica* serovar Typhimurium, one of the main foodborne pathogens responsible for human gastroenteritis.[26] The FimH proteins present on the pilli of the *Salmonella* bacteria have a high affinity for mannose units.[27,28] Our sensing scheme relies on a competitive binding of carbohydrate units and pathogen induced extraction of carbohydrates from the HC/W interface. Detection is measured by a reverse progression along the L-curve back to the original "active" state. Upon the addition of heat-killed *Salmonella enterica* serovar Typhimurium (HKST), the complex emulsions display an increase toward the maximum emission intensity (Figure 4a,b). Using B(OH)$_2$ **1**-mannan-functionalized droplets, concentration- and time-dependent monitoring of the emission intensity revealed a detection limit of $<10^4$ cells mL^{-1} recognized within less than 2 h. Interestingly, the polymeric spacer present in the B(OH)$_2$ **2** surfactant polymer allowed for a more rapid and sensitive detection of HKST cells, which was attributed to the less diffusion-hindered accessibility of these sugar-substituted complex emulsions.

The same reversible binding sensing principles were extended to a system comprising anti-*Salmonella* Typhimurium IgG antibodies, instead of mannan, to improve sensitivity and permit for higher selectivity. We opted for an oriented immobilization of the antibodies at the HC/W interface via the boronate ester binding to the N-glycans in the Fc-region of the antibody (Figure 3b).[29,30] This preferred conjugation approach leaves binding sites available for antigen binding, and it uses antibodies that have not been premodified. Reversible immobilization of antibodies at the HC/W interface requires flexibility of the surfactant and sufficient space between the interface and the B(OH)$_2$ binding sites. Thus, we used the complex emulsions functionalized with polymeric B(OH)$_2$ **2** surfactant for this study. Confocal optical micrographs of droplets functionalized with a FITC-dye labeled IgG antibody confirmed successful immobilization at the interface. Similar to the binding of carbohydrates, attachment of hydrophilic antibodies resulted in changes in the droplet morphology and thus a decrease in emission intensity with progression to the right side of the L-curve. In turn, an addition of HKST cells to these antibody-functionalized complex emulsions led to a rapid increase of the emission intensity back to the original intensity on the L-curve (blue curves in Figure 4a,b). Our results illustrated an alternative and complementary mode of rapidly (∼1 h) detecting *Salmonella* bacteria that provides the potential for portable sensors and on-site measurement with the limit of detection below 100 cell mL^{-1}. The speed and the

DOI: 10.1021/acscentsci.9b00059
ACS Cent. Sci. 2019, 5, 789−795

simplicity of our sensors made this system competitive with current methods of detecting and identifying pathogenic bacteria, such as DNA- or enzyme-based techniques, microplate culturing, and mass spectrometry, which require time-consuming enrichment steps, expensive and complicated instruments, and/or prolonged detection times.[4,7,8]

Having established the sensing capability on HKST cells, we extended our investigation toward the detection of live *Salmonella* bacteria. To anticipate the needs associated with on-site sensing platforms (e.g., simplicity, stability, and modularity), we integrated two different dyes, one in each of the droplet phases, perylene dye in the H-phase and a fluorinated perylene diimide[31] in the F-phase (Figure 4c), to allow for a calibration-free ratiometric detection. Measurement of droplets containing only a dye in the F-phase revealed slight variations in the emission intensity as a function of the morphology that can be attributed to the lens effect of the double phase emulsions.[12] By detecting the ratiometric read-out between the emission intensities of the HC-phase dye (λ = 475 nm) and the FC-phase dye (λ = 580 nm) rather than the absolute emissions, we negate size effects arising from polydisperse droplets. Figure 4d shows the sensing results of the double-dyed polydisperse emulsions with $B(OH)_2$ **2** and mannan to live *Salmonella* bacteria in phosphate-buffered saline (PBS) solution. We observed similar changes in the emission intensity as the monodisperse droplets to the HKST. Moreover, to demonstrate the applicability of our sensor in a complex protein matrix, we added live bacteria in chicken exudate into our sensing platform. We observed only minor deviations in the sensing responses between the complex protein matrix extracted from the chicken carcass and the PBS solution, and similar limits of detection were obtained within 2 h.

Safety. No unexpected or unusually high safety hazards were encountered.

CONCLUSIONS

In summary, we have demonstrated a new sensing paradigm that takes advantage of the unique chemical−structural−optical coupling in chemically functionalized fluorescent double emulsions. Specifically, we exploit the phenomenon of total internal reflection of light that was emitted in the higher refractive index hydrocarbon phase from the internal hydrocarbon/fluorocarbon interface. The emission direction of the totally internally reflected light is strongly dependent on the curvature of the internal interface and hence allows for the detection of miniscule changes in the droplet morphology. The strong correlation between experimental data and theoretical raytracing models provides for an understanding of the optical phenomena underlying the change in emission characteristics in response to droplet morphology variations. We employed stimuli-responsive boronic acid surfactants to selectively bind mono- and polysaccharides, as well as N-glycans present in IgG antibodies and the associated changes in the hydrocarbon/water interfacial tension were detected optically. These dynamic interface triggered morphology changes were used to create a rapid and sensitive method for the detection of the sugar-binding foodborne pathogen *Salmonella enterica* serovar Typhimurium. The associated understanding of the optical phenomena underlying the change in emission characteristics in response to droplet morphology variations creates a solid foundation for future detection schemes targeting other bacteria, biomacromolecules, multiplexed sensing assays, and the real-time monitoring of bacteria growth, and thereby can help to reduce food poisoning around the globe.

ASSOCIATED CONTENT

Supporting Information

The Supporting Information is available free of charge on the ACS Publications website at DOI: 10.1021/acscentsci.9b00059.

Details of experimental and computational methods and procedures (PDF)

AUTHOR INFORMATION

Corresponding Authors

*(T.M.S.) E-mail: tswager@mit.edu.
*(M.K.) E-mail: mkolle@mit.edu.

ORCID

Timothy M. Swager: 0000-0002-3577-0510

Notes

The authors declare the following competing financial interest(s): A patent has been filed on this invention.

ACKNOWLEDGMENTS

We are grateful for funding from National Institutes of Health of General Medical Sciences, Grant No. GM095843, the Jameel Water and Food Security program at MIT, and the National Science Foundation DMREF-1533985. L.Z. acknowledges support through a fellowship of the German Research Foundation (DFG) #ZE1121/1-1. S.N. and M.K. were supported in part by the U.S. Army Research Office through the Institute for Soldier Nanotechnologies at MIT, under Cooperative Agreement Number W911NF-18-2-0048. S.S. was supported by an F32 Ruth L. Kirschstein National Research Service Award. K.Y. was supported by a Funai Overseas Scholarship. Collaborative work was supported by the U.S. Department of Agriculture, Agricultural Research Service, under Agreement No. 8072-42000-084. Mention of trade names or commercial products in this publication is solely for the purpose of providing specific information and does not imply recommendation or endorsement by the USDA. The USDA is an equal opportunity employer.

REFERENCES

(1) Bhunia, A. K. *Foodborne Microbial Pathogens: Mechanisms and Pathogenesis*, 2nd ed; Springer: New York, 2018.

(2) Scallan, E.; Hoekstra, R. M.; Angulo, F. J.; Tauxe, R. V.; Widdowson, M.-A.; Roy, S. L.; Jones, J. L.; Griffin, P. M. Foodborne Illness Acquired in the United States—Major Pathogens. *Emerging Infect. Dis.* **2011**, *17*, 7−15.

(3) Hoffmann, S.; Maculloch, B.; Batz, M. *Economic Burden of Major Foodborne Illnesses Acquired in the United States. Current Politics and Economics of the United States, Canada and Mexico*, U.S. Department of Agriculture, Economic Research Service: Washington, DC, 2015, *17*, pp 543−616.

(4) Váradi, L.; et al. Methods for the Detection and Identification of Pathogenic Bacteria: Past, Present, and Future. *Chem. Soc. Rev.* **2017**, *46*, 4818−4832.

(5) Doyle, M. P.; Buchanan, R. L. *Food Microbiology: Fundamentals and Frontiers*; American Society for Microbiology Press: Washington, DC, 2012.

(6) Carlson, K.; Misra, M.; Mohanty, S. Developments in Micro-and Nanotechnology for Foodborne Pathogen Detection. *Foodborne Pathog. Dis.* **2018**, *15*, 16−25.

DOI: 10.1021/acscentsci.9b00059
ACS Cent. Sci. 2019, 5, 789−795

(7) Alahi, M. E. E.; Mukhopadjyay, S. C. Detection Methodologies for Pathogens and Toxins: A review. *Sensors* **2017**, *17*, 1885−1905.
(8) Ahmed, A.; Rushworth, J. V.; Hirst, N. A.; Millner, P. A. Biosensors for Whole-Cell Bacterial Detection. *Clin. Microbiol. Rev.* **2014**, *27*, 631−646.
(9) Zarzar, L. D.; et al. Dynamically Reconfigurable Complex Emulsions via Tunable Interfacial Tensions. *Nature* **2015**, *518*, 520−524.
(10) Choi, C. H.; Weitz, D. A.; Lee, C. S. One Step Formation of Controllable Complex Emulsions: From Functional Particles to Simultaneous Encapsulation of Hydrophilic and Hydrophobic Agents into Desired Position. *Adv. Mater.* **2013**, *25*, 2536−2541.
(11) Zarzar, L. D.; Kalow, J. A.; He, X.; Walish, J. J.; Swager, T. M. Optical Visualization and Quantification of Enzyme Activity using Dynamic Droplet Lenses. *Proc. Natl. Acad. Sci. U. S. A.* **2017**, *114*, 3821−3825.
(12) Zhang, Q.; et al. Emulsion Agglutination Assay for the Detection of Protein-Protein Interactions: An Optical Sensor for Zika Virus. *ACS Sensors* **2019**, *4*, 180−184.
(13) Nagelberg, S.; et al. Reconfigurable and Responsive Droplet-based Compound Micro-lenses. *Nat. Commun.* **2017**, *8*, 14673.
(14) James, T. D.; Sandanayake, K. R. A. S.; Shinkai, S. Chiral Discrimination of Monosaccharides using a Fluorescent Molecular Sensor. *Nature* **1995**, *374*, 345−347.
(15) Wu, X.; et al.et al Selective Sensing of Saccharides using Simple Boronic Acids and their Aggregates. *Chem. Soc. Rev.* **2013**, *42*, 8032−8048.
(16) Axthelm, J. R.; et al. Fluorinated Boronic acid-appended Pyridinium Salts and ^{19}F-NMR Spectroscopy for Diol Sensing. *J. Am. Chem. Soc.* **2017**, *139*, 11413−11420.
(17) Bull, S. D.; et al. Exploiting the Reversible Covalent Bonding of Boronic acids: Recognition, Sensing, and Assembly. *Acc. Chem. Res.* **2013**, *46*, 312−326.
(18) Matsumoto, A.; Sato, N.; Kataoka, K.; Miyahara, Y. Noninvasive Sialic Acid Detection at Cell Membrane by using Phenylboronic acid Modified Self-assembled Monolayer Gold Electrode. *J. Am. Chem. Soc.* **2009**, *131*, 12022−12023.
(19) Zhang, Q.; et al. Facile Bottom-up Synthesis of Coronene-based 3-fold Symmetrical and Highly Substituted Nanographenes from Simple Aromatics. *J. Am. Chem. Soc.* **2014**, *136*, 5057−5064.
(20) Chen, P.-C.; Wan, L.-S.; Ke, B.-B.; Xu, Z.-K. Honeycomb-patterned Film Segregated with Phenylboronic acid for Glucose Sensing. *Langmuir* **2011**, *27*, 12597−12605.
(21) Lorand, J. P.; Edwards, J. O. Polyol Complexes and Structure of the Benzeneboronate Ion. *J. Org. Chem.* **1959**, *24*, 769−774.
(22) James, T. D.; Sandanayake, K.; Shinkai, S. Saccharide Sensing with Molecular Receptors based on Boronic Acid. *Angew. Chem., Int. Ed. Engl.* **1996**, *35*, 1910−1922.
(23) Lis, H.; Sharon, N. Lectins: Carbohydrate-Specific Proteins that Mediate Cellular Recognition. *Chem. Rev.* **1998**, *98*, 637−674.
(24) Disney, M. D.; Zheng, J.; Swager, T. M.; Seeberger, P. H. Detection of Bacteria with Carbohydrate-Functionalized Fluorescent Polymers. *J. Am. Chem. Soc.* **2004**, *126*, 13343−13346.
(25) Karlsson, K.-A. *Bacterium-Host Protein-Carbohydrate Interactions and Pathogenicity*; Portland Press Limited, 1999.
(26) McClelland, M.; et al. Complete Genome Sequence of Salmonella Enterica Serovar Typhimurium LT2. *Nature* **2001**, *413*, 852−856.
(27) Kisiela, D.; et al. Functional Characterization of the FimH Adhesin from Salmonella Enterica Serovar Enteritidis. *Microbiology* **2006**, *152*, 1337−1346.
(28) Lin, C.-C.; et al. Selective Binding of Mannose-Encapsulated Gold Nanoparticles to Type 1 Pili in Escherichia Coli. *J. Am. Chem. Soc.* **2002**, *124*, 3508−3509.
(29) Duval, F.; Van Beek, T. A.; Zuilhof, H. Key Steps towards the Oriented Immobilization of Antibodies using Boronic Acids. *Analyst* **2015**, *140*, 6467−6472.
(30) Lin, P.-C.; et al. Fabrication of Oriented Antibody-Conjugated Magnetic Nanoprobes and Their Immunoaffinity Application. *Anal. Chem.* **2009**, *81*, 8774−8782.
(31) Yoshinaga, K.; Swager, T. M. Fluorofluorescent Perylene Bisimides. *Synlett* **2018**, *29*, 2509−2514.

DOI: 10.1021/acscentsci.9b00059
ACS Cent. Sci. 2019, 5, 789−795